Chapter 2. Simulation of the Mat Formation Process

Summary

The parameters of the manufacturing process have a substantial effect on the final mechanical and physical properties of wood-based composites. The number of interacting variables during the production process is prohibitively large to assess a wide variety of data by experimental means. A combined stochastic and deterministic model, based on fundamental engineering principles, was developed and validated for establishing the critical relationships between the processing parameters and the physical properties of oriented strandboard (OSB). In the first phase of this research a Monte Carlo simulation model was developed for describing the spatial structure of three-layer OSB. The model was designed to mimic the strand deposition during the mat formation, including the three-dimensional spatial geometry, orientation and density of the strands. These physical characteristics of the mat formation process were considered as stochastic variables that can be described by well developed probability distributions. The parameters of these underlying distributions were derived from data collected on industrial strands by using an image analysis technique. The model superimposes a grid on the simulated mat and is capable of computing the number of strands, as well as the thickness and density of the mat, at each grid point. Additionally, it can predict the change in several void volume fractions and strand contact area within the mat during the consolidation. The model has application to wafer, particle, and fiber mats as well. This structural simulation model is the basis of further model development that describes the heat and mass transfer processes, and the viscoelastic nature of the hot-pressing operation during OSB manufacturing.

2.1 Introduction

The hot-pressing process is one of the critical stages during the production of wood-based composites. A loosely formed mat is compressed to its final thickness under elevated pressure and temperature. Several interacting physical phenomena occur during the consolidation that influence the final properties of the product. At the initial stage of the hot-pressing, the bound water content of the wood elements evaporates as the temperature increases abruptly at the surface of the mat close to the hot press platens. The evaporation builds up a substantial vapor pressure, which drives the vapor to the colder core of the mat, where it may condense. As the core temperature gradually increases, the water content of the core also vaporizes, and the increased pressure drives the vapor to the edge of the mat, where it leaves the structure. The moisture transport declines as the water content of the wood elements nears depletion. Meanwhile, the heat transport is assisted by the steam flow and subsides as the mat temperature approaches the press platen temperature. Therefore, a dynamic water and heat transport can be observed during the hot-pressing operation. The rate of the moisture and heat transfer strongly depends on the structure of the mat, and how this structure changes during the compression. More precisely, the transient void volume, which is comprised of the gaps between the wood elements, provides the pathway to fluid flow and is directly linked to the changing heat and mass transfer properties (thermal conductivity, permeability, diffusivity) of the mat during the consolidation process. Furthermore, the voids in the uncompressed mat structure are a function of the size and geometry of the wood elements. Smaller and more uniform sized elements will form smaller voids. In the case of larger elements, such as strands or wafers, a considerable amount of void might develop in the mat due to tilting and bridging of the constituents. Accordingly, it is quite important that the initial value, and the characteristic change of the void volume, is properly predicted by the mat formation model, and it must be incorporated in the heat and mass transfer simulation. The primary goal of the first phase of this research was to develop a simulation process that adequately describes the spatial structure of OSB mats and can handle the change in void volume and strand contact area during the press closure.

2.2 Background

Quantitative understanding of the mat formation process used in the manufacture of wood-based composites can help to establish structure and property relationships. Researchers have realized the importance of the structural characterization in relation to the final quality of wood-based composite products (Lang and Wolcott 1995, Kallmes 1961, Kallmes and Corte 1960, Kallmes et al. 1961, Suchsland 1959, 1962, Steiner and Dai 1993). One of the earliest papers that describes the structure and property relationships of particleboard was published by Suchland (1959). He investigated the effect of particle geometry on the initial void volume and the resulting horizontal density distribution within the mat. He also recognized that the bending stiffness of the board is not only a function of final board density, but also depends on the degree of contact of particles during the compression (Suchsland 1962, 1967). Suchsland also described the horizontal density variation using a veneer strip model (Suchsland and Xu 1989, Suchsland and Hong 1989). This model was based on several mutually perpendicular layers of uniform size veneer strips, including air gaps, bonded together in a board. The strips could overlap, forming a horizontal density distribution within the mat. The number of overlaps was a good indicator to internal bond strength and thickness swelling characteristics.

Two basic computer simulation modeling approaches were developed to characterize the spatial structure of randomly formed wood flake composites: the surface and the edge models. The surface model (Dai and Steiner 1993, 1994a, 1994b, Steiner and Dai 1993) incorporates geometric probability theory and simulation techniques for describing the characteristics observable on the surface of the flake mat. The basis of the model is an idealized, randomly formed, flake layer network, where the dimensions of the flakes are uniform, and the number of the flakes is limited in a manner that the sum of the area of the flakes is equal to the area of the layer. Given these assumptions, several properties of the flake network became mathematically definable using probability distributions, and a random field theory. The composite mat is constructed from these single layers of flakes. The model can calculate the horizontal density distribution of the mat, the flake-to-flake contact area, and the void volume fraction. Furthermore, it can predict the stress-strain behavior of the mat based on the transverse compression properties of cellular solids.

The edge model (Lang and Wolcott 1995, 1996a, 1996b) subdivides the mat into imaginary flake columns of finite size. The geometrical properties of the columns are determined by experiments and measured at the edge of the mat. Probability density functions are then fit to the data. The columns are reproduced by sampling the fitted probability distributions with the simulation model. This model predicts stress development due to flake bending at the early stage of the mat consolidation in addition to the transverse compression of the flakes at higher pressures. Good agreement was found between predicted and measured compression stress

values at stress level as low as 0.01 MPa, which is important in manufacturing low density composite panels.

The above mentioned mat formation models were developed using constant flake geometry and completely random orientation of the flakes. However, the flake geometry has a definite relationship with packing efficiency, and thus it will influence the density of the composite (Kelley 1977, Brumbaugh 1960, Bhagwat 1971, Heebink and Hann 1959, Strickler 1959, Hoglund et al. 1976). In the case of the formation of certain wood-based composite mats, such as oriented strand board and oriented strand lumber, the orientation of the strands is also restricted. Although the measurements of the number of overlapping strands and strand orientation is relatively simple, for more refined wood-based composites, such as particle and fiber mats, the measurements would be far more challenging.

In order to improve on the predictions of the previous models, a more realistic description of the mat structure was developed, where the mat formation includes the geometry of the wood elements as random variables and certain limitations can be imposed on the orientation of the elements. Additionally, a density value is assigned to each individual strand, allowing the simulation of the horizontal density distribution of composites made out of mixed species. The model was developed based on data obtained from commercial strand measurements and the mat formation process model was validated by comparison of the simulated horizontal density distribution to a measured horizontal density distribution. At the present time, none of the published models could predict the real structure and horizontal density distribution of a commercial, three-layer OSB mat, based on geometry and density measurements on industrial strands.

2.3 Model Development

2.3.1 General Model Development

Over the years several stochastic models were developed for describing the spatial characteristics of wood-strand mats (Dai and Steiner 1993, 1994a, 1994b, Lang and Wolcott 1995, 1996a, 1996b). These models had specific purposes either to describe the stress-strain behavior of the mat during the consolidation process or to simulate other relevant manufacturing parameters. In this research a numerical description of the spatial structure of three-layer OSB mat was needed to further investigate the heat and mass transfer phenomenon. The approach included the stochastic nature of dimensions, orientation and density of the constituents during the mat formation process. The general idea of the mat formation simulation was to virtually reconstruct the mat from individual wood elements. The characteristics of the deposition and strand dimensions were obtained from experimentally determined probability distributions. The best fitting distributions were sampled by the simulation routine with algorithms described by Law and Kelton (1982). In order to make the model viable to describe the transient processes during the press closure, the general model was divided into three main parts.

In the first part, the mat formation process was simulated by numerically depositing random sized strands in a predetermined mat area, as detailed in computational flow chart shown in Figure 2.1. This process required input values, such as the number of layers and the cumulative mass of the strands deposited at each layer. Model assumptions include: strands are parallel to the base of the mat, strands have an approximated rectangular shape, the strand deposition follows a standard uniform distribution (equal chance for each strand to drop anywhere within the predetermined mat area), the orientation of the strands follows a uniform distribution within experimentally determined limits, and the probability distributions of the strand dimensions (length, width, thickness) are based on samples representing the population distributions by layers.

The model can generate any size mat, but at the edges the simulation is not representative, because strands which are partly outside of the predetermined boundaries, will not be present at the edges, creating unjustified voids along the perimeter of the predetermined mat area. Other researchers addressed this problem using the torus convention (Dai and Steiner 1993, 1994a, 1994b, Lang and Wolcott 1995, 1996a, 1996b), that states that part of the strand protruding out from the predetermined mat area is reentering on the other side as a partial strand. However, due to computational difficulties, this routine can not be applied easily to describe the mat forming process. Instead, the problem can be solved by trimming the edges of the simulated mat by an amount equal to the size of the average strand length.

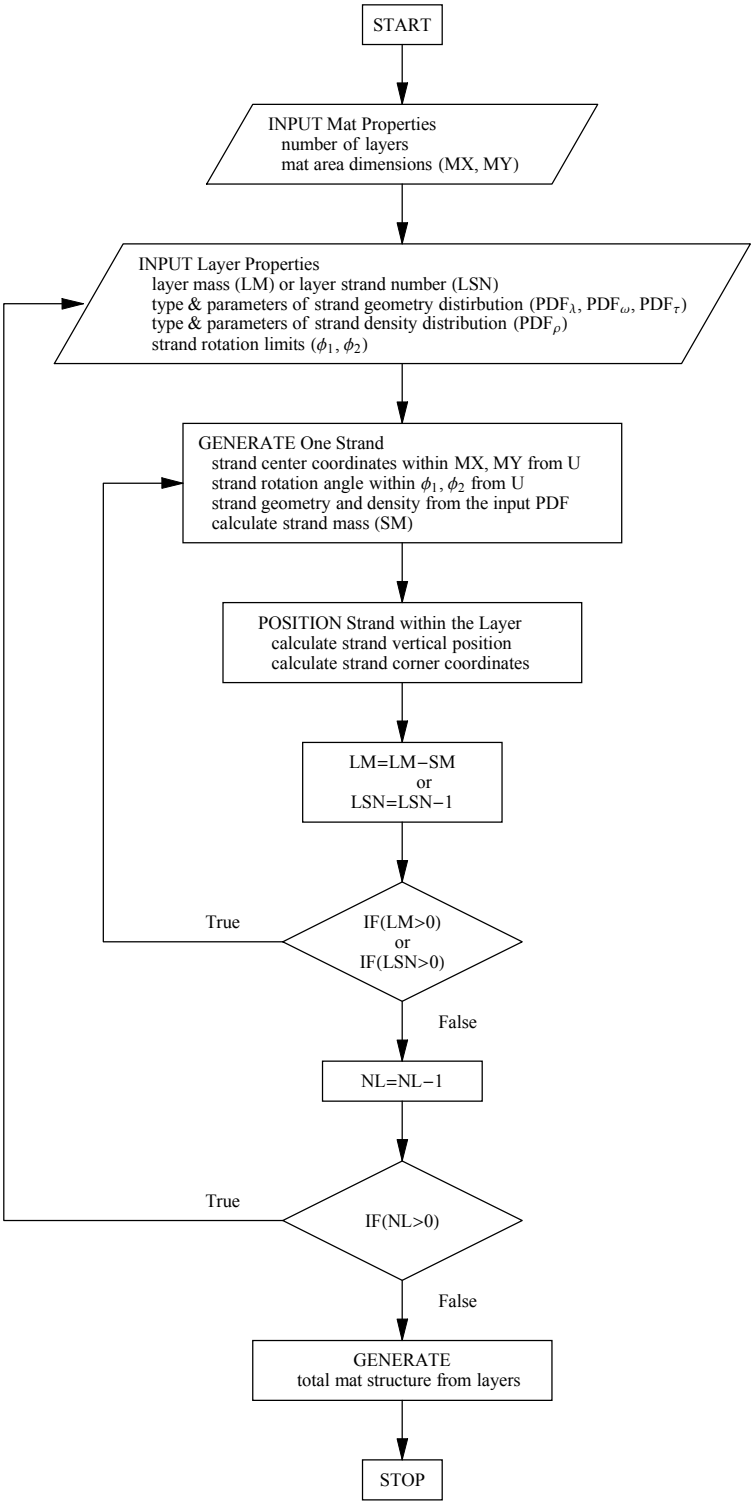

Figure 2.1. Flow diagram of the mat reconstruction routine.

This simulation routine is governed by the target final density of the panel. From this predetermined physical property the necessary total mass of strands is computed. When the generated cumulative mass of the strands reaches this value, the simulation process ends.

In the second stage of the simulation, a grid is superimposed over the valid area of the mat. The grid establishes imaginary strand columns, in which the number, the cumulative thickness and mass of the strands are calculated and stored. The strand counter algorithm allows for the superposition of virtually any sized grid over the mat area in question. However, due to computer processing time, the maximum resolution of the investigated mat area is about 200,000 imaginary columns. Figure 2.2 describes the general computational flow chart of this process.

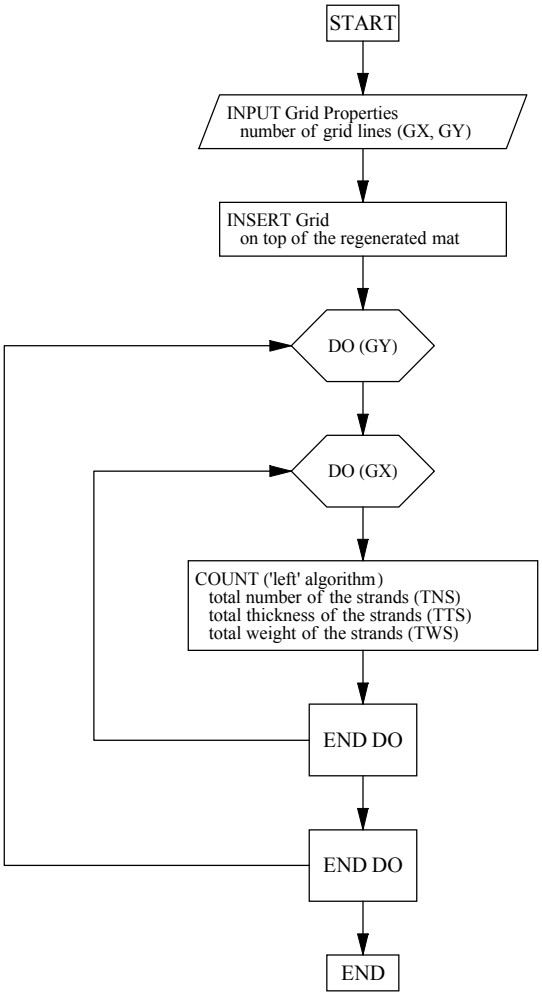

Figure 2.2. Flow diagram of the mat property calculations (GX and GY are grid points in the x and y directions).

Two approaches to the computational geometry problem imposed by the strand counter algorithm were considered. The first is the “triangulation” method, where the vertices of the polygon (in-plane shape of the strand) are connected to the grid point, forming triangles. Whenever the sum of the areas of the triangles is equal to the area of the polygon, the point is inside the polygon (Figure 2.3a). However, when the total area of the triangles is larger than that of the rectangular area of the strand, then the point is outside of the polygon, thus it is not counted (Figure 2.3b). Although this method is easy to implement, it has a practical limitation. The areas can be calculated and compared with a certain digital precision. The program can make a wrong decision whenever the point is too close to the side of the polygon. In this case the difference between the sum of the areas of the triangles and the area of the polygon is zero according to digital precision. The routine substantially slows down as the precision is refined.

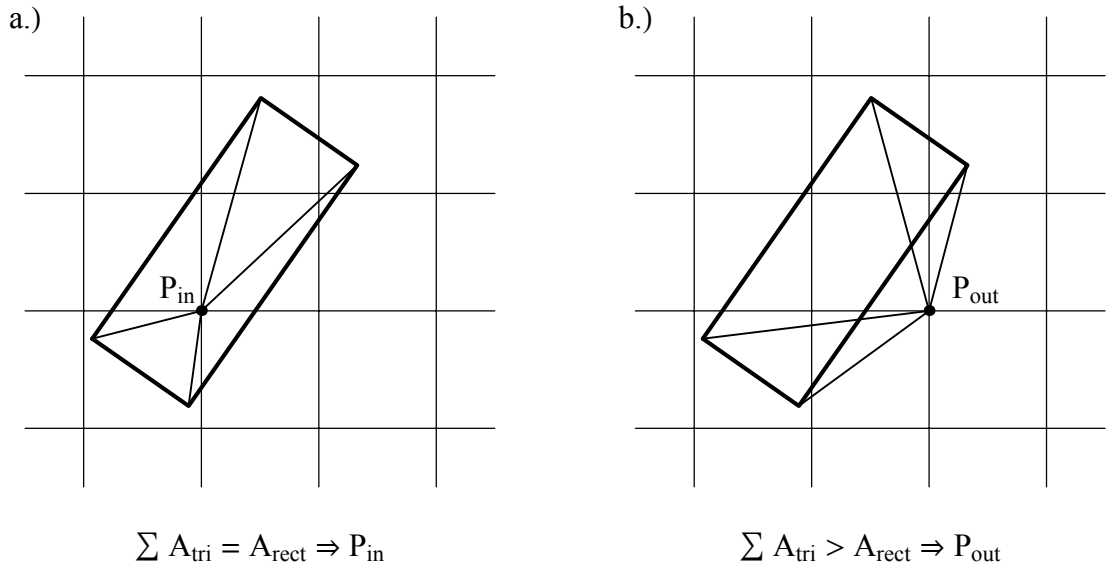

Figure 2.3. Decision rule of the "triangulation" algorithm.

The second approach, finally implemented in the model, is referred to as the “left” algorithm (O’Rourke 1994). Essentially the routine “walks” around the perimeter of the polygon (strand) counterclockwise, meanwhile looking at the point. Whenever the grid point is inside of the strand, it always appears at the left side during the walk. However, the point appears sometimes at the right side, if it is outside of the strand (Figure 2.4). Additionally, if the point is positioned at the boundary of the polygon, the algorithm will walk through it, which allows grid points to be positioned at the perimeter of the strands.

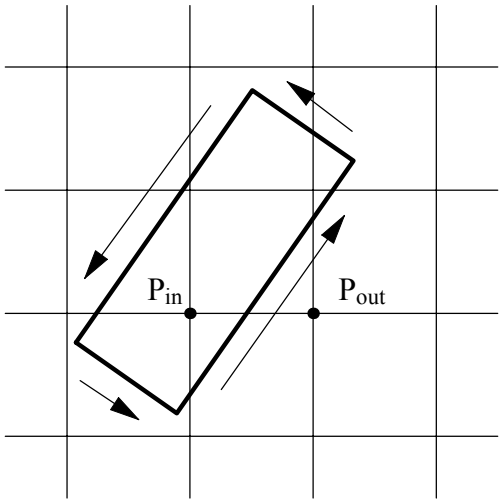

Figure 2.4. Decision rule of the "left" algorithm.

For the simulation of transient effects during the press closure, the third part of the model virtually describes the press platen closure during a cold pressing process (Figure 2.5). At this stage of the model development, there was no interest to describe the stress-strain relationships during the compression process since the mechanical properties are dependent on temperature and moisture content. The current analysis is concerned only with the structural changes that occur during the compression of the mat. This part of the routine starts the consolidation process from a specified mat thickness. The mat thickness depends on the target thickness and target density of the final panel. The routine calculates the void volume between strands and the void volume within strands in each imaginary column continuously during the consolidation, as well as the strand contact areas as a function of time. The model has the flexibility to simulate real press closing schedules, including the press closing time and venting periods. The strand contact area is a good indicator of the effective bonded area (Dai and Steiner 1994a). The calculations are based on the cumulative thickness of the strands in the imaginary strand columns relative to the distance between the press platens. Whenever the cumulative thickness is less than the distance between the platens, the strands are not in contact and void volume exists.

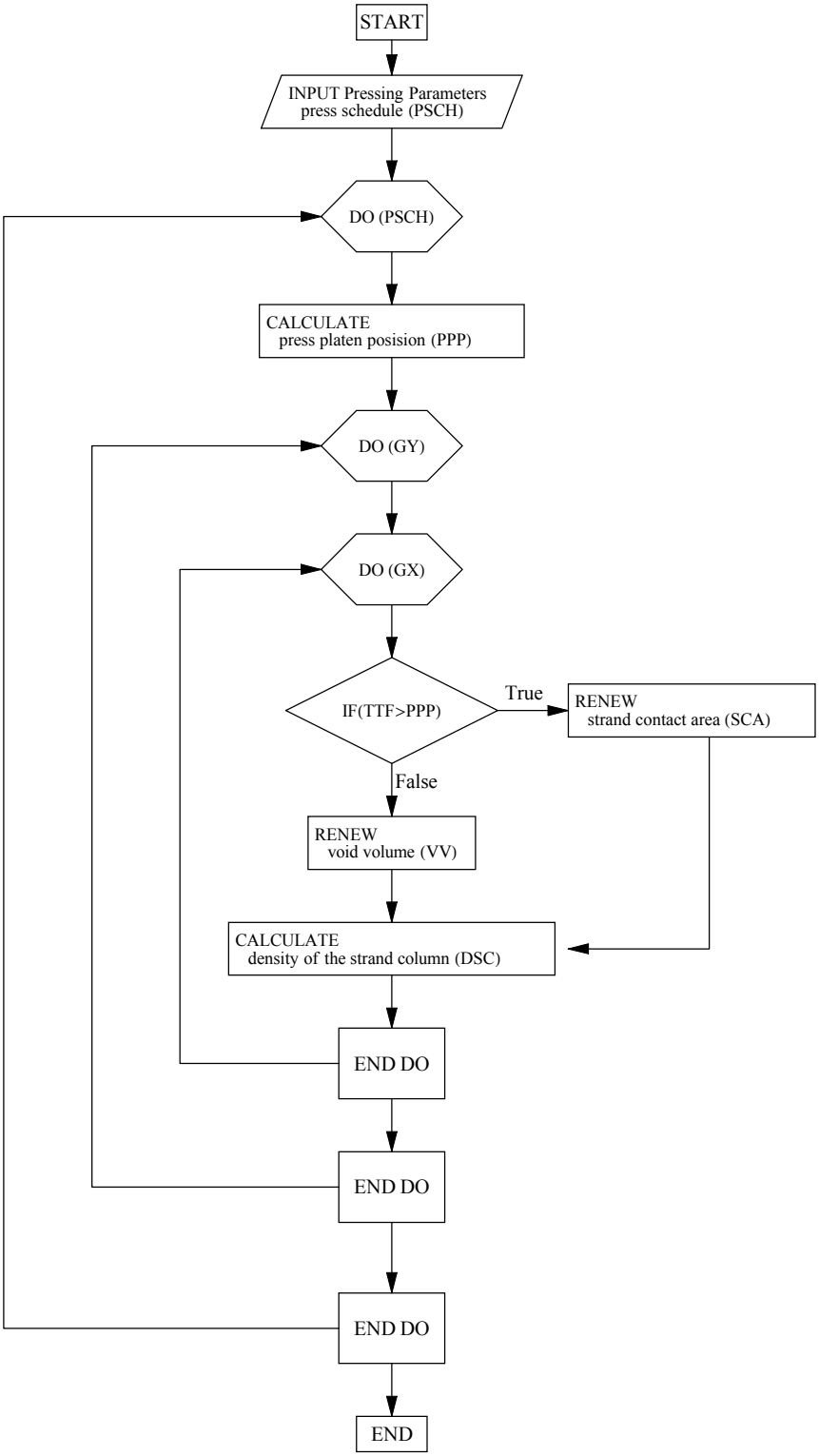

Figure 2.5. Flow diagram of the press closing simulation.

2.3.2 Monitoring Structural Changes of the Mat during Compression

A double cellularity can be identified within the structure of the mat. Space exists among the strands due to the inherent randomness of the deposition process (between flake void), and the flakes include the cell lumen in their structure (within flake void). Consequently, it is possible to distinguish not only two different voids, but also two different densities: the density of the mat (ρ_m), and the average density of the component flakes (ρ_f). At the beginning of the press closure only the between flake void (V_s) is eliminated from the mat structure, resulting in only a density increase of the mat. As the between flake voids are eliminated and the flakes make contact, further pressure increase collapses the cell wall, and the lumen volume is decreased (V_l). At this stage both the density of the mat, and the density of the constituent flakes has increased. The change of the magnitude of the two types of voids (space and lumen) in the mat structure, together with the two types of densities (mat and flake) can be monitored by the mat formation model. The calculations are based on the following considerations.

The volume of the mat (V_m) is the sum of the volume of the flakes (V_f) and the volume of the space (V_s):

$$V_m = V_f + V_s. \tag{2.1}$$

The volume of the flakes can be further subdivided into volume of the cell wall (V_{cw}) and volume of the lumens (V_l):

$$V_f = V_{\mathrm{cw}} + V_l. \tag{2.2}$$

The total void volume within the mat structure (V_v) is given as:

$$V_v = V_s + V_l. \tag{2.3}$$

The mat formation model can calculate the change of the volume of the mat and the volume of the space during the compression process, and also the total mass of the flakes (m_f). Knowing these values, density relationships can be derived, such as the density of the mat

$$\rho_m = \frac{m_f}{V_m}, \tag{2.4}$$

and the density of the flakes

$$\rho_f = \frac{m_f}{V_f}. \tag{2.5}$$

The model also calculates fractional void volumes, such as the lumen fraction within the flakes (ζ_{lf}):

$$\zeta_{\mathrm{lf}} = \frac{V_l}{V_f} = 1 - \frac{\rho_f}{\rho_{\mathrm{cw}}}, \tag{2.6}$$

where

ρ_{cw} = cell wall density.

The space fraction within the mat (ζ_{sm}):

$$\zeta_{\mathrm{sm}} = \frac{V_s}{V_m}, \tag{2.7}$$

the lumen fraction within the mat (ζ_{lm}):

$$\zeta_{\mathrm{lm}} = \frac{V_l}{V_m} = \zeta_{\mathrm{lf}} (1 - \zeta_{\mathrm{sm}}), \tag{2.8}$$

and the total void fraction within the mat (ζ_{vm}):

$$\zeta_{\mathrm{vm}} = \frac{V_v}{V_m} = \frac{V_l + V_s}{V_m} = \zeta_{\mathrm{lm}} + \zeta_{\mathrm{sm}} = \zeta_{\mathrm{lf}} (1 - \zeta_{\mathrm{sm}}) + \zeta_{\mathrm{sm}}. \tag{2.9}$$

The structural change of the mat, described by the densities and void fractions, has a crucial effect on the physical and transport properties during the consolidation. This has to be taken into consideration in the heat and mass transfer part of the hot-compression model, especially when the press closing process is simulated.

2.4 Materials and Methods

2.4.1 Database Assessment for Input Values of the Model

The first part of the simulation routine required spatial geometry of face and core strands as well as density distribution of the constituents. Strands from the face and core layers of OSB were obtained from a commercial facility. The furnish included a mixture of softwood and hardwood, primarily southern pine (*Pinus spp.*) and yellow-poplar (*Liriodendron tulipifera*). The average moisture content was 6 %.

The length, width, and thickness distributions of the strands were assessed using an image analysis system, which consisted of a black and white video camera, macro lens, frame grabber board, and image analysis software (ImagePro3.0). Approximately 1,700 core and surface strands were randomly sampled and analyzed by the system. The sample sizes represented all size fractions of the strands. Figure 2.6 shows the typical size and shape of face layer strands.

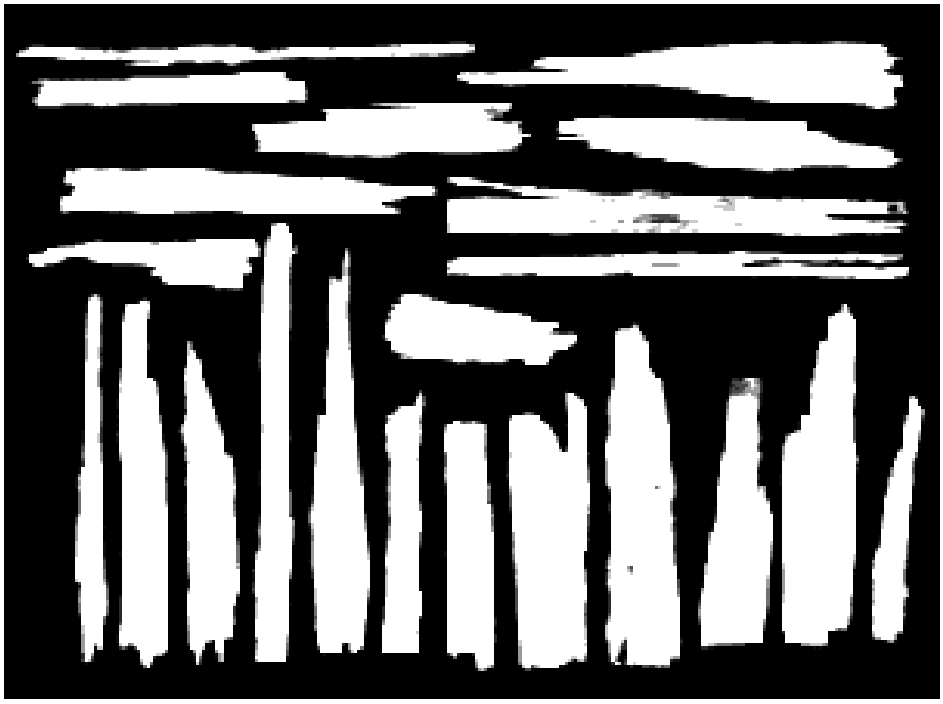

Figure 2.6. Typical digital image of face layer strands captured by the image analysis system.

By measuring the area and perimeter of the irregular shaped strands, an apparent length and width could be calculated. This process assumes that the area and perimeter of the resulting rectangle are equal to the area and perimeter of the original strands. Numerically, the computations are defined by the following equations

$$l = \frac{P + \sqrt{P^2 - 16A}}{4}, \tag{2.10}$$

$$w = \frac{P - \sqrt{P^2 - 16A}}{4}, \tag{2.11}$$

where

l = apparent length (mm),
w = apparent width (mm),
P = perimeter of the strand (mm),
A = area of the strand (mm^2) .

Preliminary measurement showed that there was no significant difference between two thickness measurements at the third points along the length of the strands. Therefore, the thickness of each strand was manually measured at the midpoint by a digital caliper with an accuracy of 0.01 mm. The weight of each strand was measured by a digital scale having an accuracy of 0.01 g. From these measurements the density of each strand was determined.

The above described measuring technique provided an adequate sample size (n > 800) that was used to establish the probability distribution functions of each variable in question. Commercial software (Stat::Fit 1.10.06.2, Geer Mountain Software) was used for determining the type and parameters of the best probability density functions that fit the data. Standard statistical procedures, including goodness-of-fit tests (Chi-square, Kolgomorov-Smirnoff), were used to confirm that the experimentally observed measurements could have come from the specified probability distribution.

2.4.2 Experimental Validation of the Model

For validation of the model, simulated and actual horizontal density distributions of single layer, random-oriented strand boards were compared. Liquid phenol-formaldehyde resin, 4 % by weight, was sprayed on the face strands obtained from the same OSB mill. Five 610 x 610 mm mats were hand-formed and compressed to 19 mm final thickness (~ 24 inch x 24 inch x 0.75 inch) in a hot press at a 200 °C platen temperature. The dry target density of the boards was 610 kg/m^3 (~38 lb/ft^3). The boards were trimmed to 450 x 450 mm dimensions and then cut into 30 mm squares. The density of the 30 mm square blocks was calculated by measuring the dimensions and the weight of the blocks. Using the average measured board density, five simulations were run and the horizontal density distributions were obtained. The simulated compressed mat was subdivided into 30 mm dimension blocks. The average of 81 densities, calculated at grid points 3.75 mm apart, was used to determine the density of each block, which resulted in a simulated horizontal density profile. Standard statistical procedures were used to compare the means of the simulated and experimentally obtained densities.

2.5 Results and Discussion

2.5.1 General Characteristics and Probability Density Functions of the Input Variables

The summary statistics of the density and spatial geometry of the face and core layer strands are presented in Table 2.1. The mean of the measured strand properties were compared by paired t-tests for statistically significant differences. The density of the strands in the core and face layers were not significantly different at the 90 % confidence level, which is reasonable, considering that no effort was made by the company to separate species for the different layers of the mat. However, the measurements revealed that there was a significant difference between the geometry of the face and core strands. The face strands tended to be longer, wider and thicker than strands in the core. This fact is attributed to the industrial screening practice, which intentionally separates the strands based on length and width. Consequently, the investigation of possible distribution functions of these variables should be separated by core and face. Table 2.2 compiles the results of these probability fitting procedures. The width, thickness and density followed the three-parameter Gamma distribution. Two types of standard goodness-of-fit tests were performed on the data. The Kolgomorov-Smirnoff test at 95 % confidence level confirmed that these variables came from the specified probability distributions. However, the Chi-square test did not confirm the distribution concerning the thickness of the face strands. Nevertheless, the three-parameter Gamma distributions were used for generating the above variables for simulation purposes, because of the lack of a better fitting statistical distribution. Figures 2.7 through 2.9 show the histograms of the experimental data overlaid with the best fitting probability density function.

Table 2.1. Descriptive statistics of core and face layer strand properties.

		Length [mm]	Width [mm]	Thickness [mm]	Density [kg/m^3]	Area [mm^2]	Perimeter [mm]
CORE	Mean (μ)	53.93	6.19	0.59	474	373.81	120.23
n = 851	Stdev.(σ)	27.12	3.51	0.22	74	376.81	57.57
	C.O.V. [%]	50.30	56.76	37.39	15.60	100.80	47.88
	Min	9.50	0.87	0.15	310	37.85	28.85
	Max	133.41	25.92	1.60	735	3188.30	297.82
FACE	Mean (μ)	78.44	8.87	0.64	466	744.33	174.62
n = 834	Stdev.(σ)	25.42	5.23	0.21	73	581.55	55.53
	C.O.V. [%]	32.41	58.98	32.96	15.54	78.13	31.80
	Min	12.89	1.20	0.13	352	54.79	34.76
	Max	165.45	39.63	1.62	684	4043.96	354.28

Table 2.2. Results of the goodness-of-fit tests. The tests were performed with 95% confidence level (α_{stat}=0.05).

	Flake Variables	Fitted Distribution	Parameters			Goodness-of-Fit Statistics						
			min.	α	β	d.o.f.**	χ^{2***}	χ^2 (α_{stat}, d.o.f.)	p-value+	K-S****	K-S (α_{stat}, n)	p-value+
CORE	Length [mm]	Empirical	---	---	---	---	---	---	---	---	---	---
n=851	Width [mm]	Gamma	0.788	2.495	2.165	11	16.60	19.70	0.120	0.0269	0.0464	0.557
	Thickness [mm]	Gamma	0.015	6.807	0.085	11	18.60	19.70	0.069	0.0301	0.0464	0.412
	Density [kg/m^3]	Gamma*	310.000	4.728	34.671	11	13.00	19.70	0.291	0.0313	0.0464	0.364
FACE	Length [mm]	Empirical	---	---	---	---	---	---	---	---	---	---
n=834	Width [mm]	Gamma	1.085	2.280	3.415	11	9.77	19.70	0.551	0.0179	0.0468	0.949
	Thickness [mm]	Gamma	0.000	8.690	0.074	11	24.30	19.70	0.011	0.0412	0.0468	0.115
	Density [kg/m^3]	Gamma*	351.000	2.340	49.329	11	9.91	19.70	0.538	0.0214	0.0468	0.831

* = fixed lower bound

** = number of intervals

*** = equal probable interval

**** = Kolgomorov-Smirnoff goodness-of –fit test

\+ = level of significance of the goodness-of-fit test (has to be larger than 0.05 to accept the null hypothesis, that the PDF provides a good fit to the data)

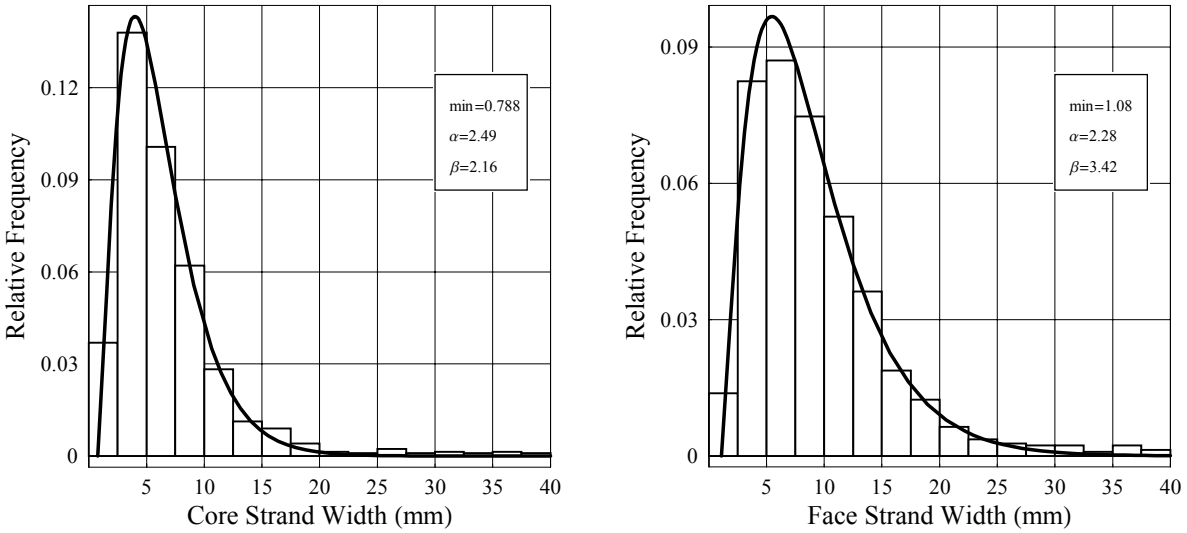

Figure 2.7. Frequency histogram of core and face layer strand width. The fitted three-parameter Gamma distribution is overlaid.

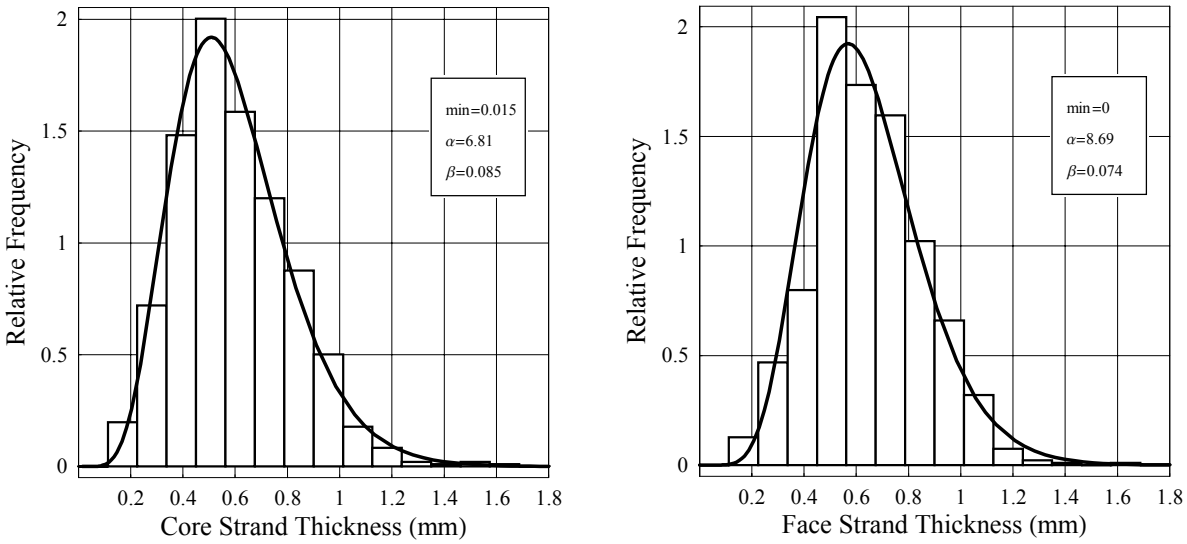

Figure 2.8. Frequency histogram of core and face layer strand thickness. The fitted three-parameter Gamma distribution is overlaid.

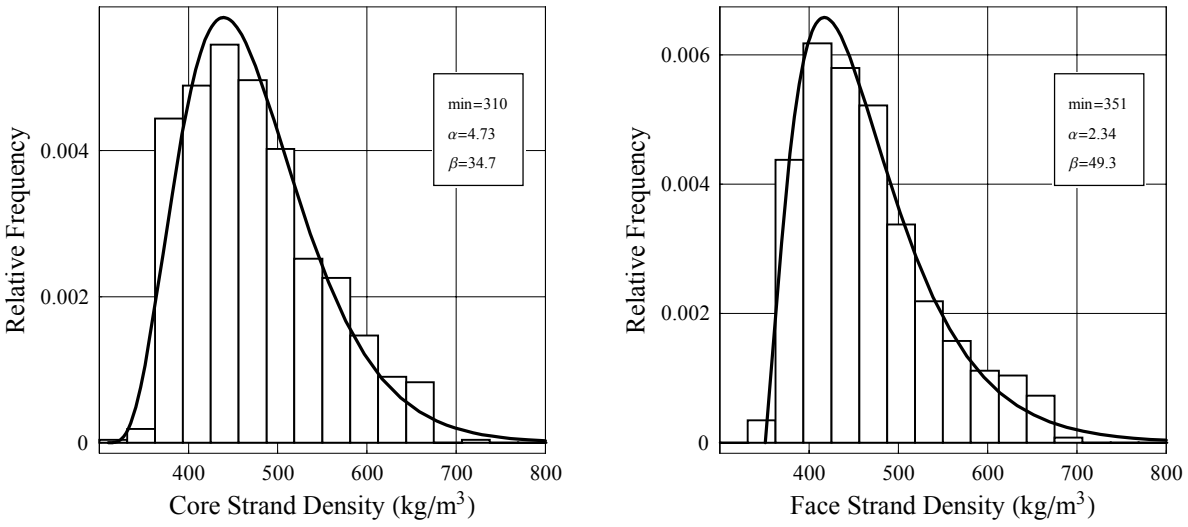

Figure 2.9. Frequency histogram of core and face layer strand density. The fitted three-parameter Gamma distribution is overlaid.

Several probability density functions were fit to the strand length data. However, none of the probability distribution functions provided an adequate fit to the longitudinal dimension of the strands. There were two noticeable peaks in the frequency histograms at approximately 50 and 100 mm lengths (Figure 2.10).

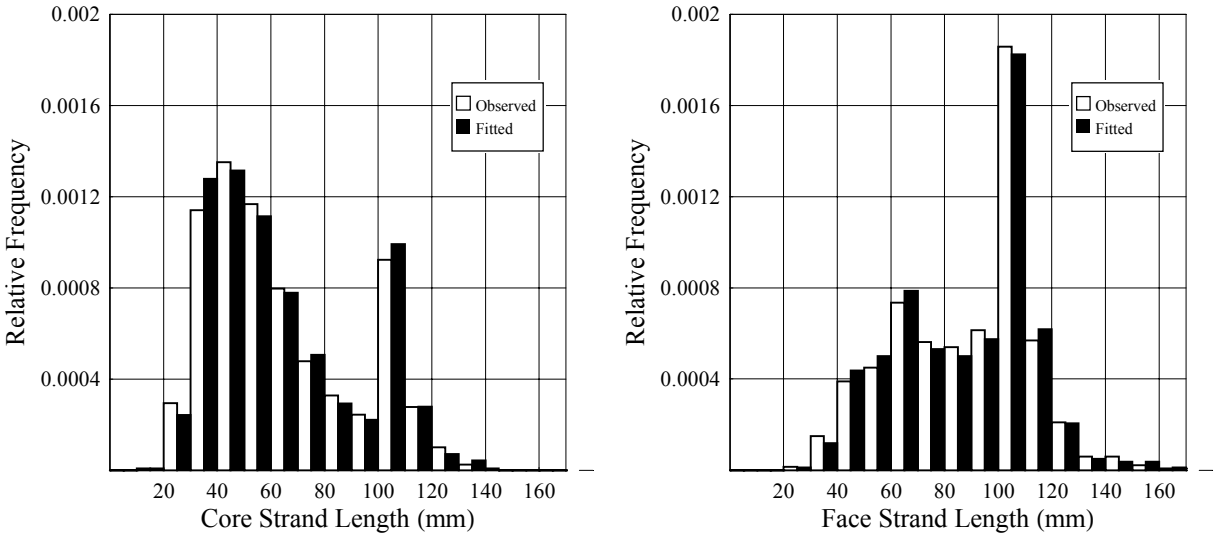

Figure 2.10. Frequency histogram of core and face layer strand length. The results of the simulation of 1000 strand length from the empirical distribution is also depicted.

The core flakes have the second peak because some of the 100 mm target length face flakes pass through the screens. Repeated measurements of the length confirmed the existence of the two peaks. Consequently, an empirical distribution was used to describe the length data. The procedure groups the data and calculates the cumulative distribution from the number of observations in each group. The resulting cumulative distribution was then sampled by uniform random numbers. The details of the empirical fitting procedure is described by Law and Kelton (1982).

There is a subtlety involving Figures 2.7 and 2.10. The measured quantities were area (A) and perimeter (P), from which widths (w) and lengths (l) were inferred assuming perfectly rectangular flakes. Figures 2.7 and 2.10 show the distributions for these calculated quantities w and l. Since the flakes are not truly rectangular, however, it is not obvious that generating length and width according to the inferred distributions will yield distributions of area and perimeter that match the observed distributions. Figure 2.11 shows, for the face, the measured area and perimeter distributions versus the distributions of $A = l \cdot w$ and $P = 2 (l + w)$ obtained by sampling w and l from the inferred distributions in Figures 2.7 and 2.10. The close agreement of the measured and calculated area and perimeter data assured the adequacy of the strand geometry transformation procedure.

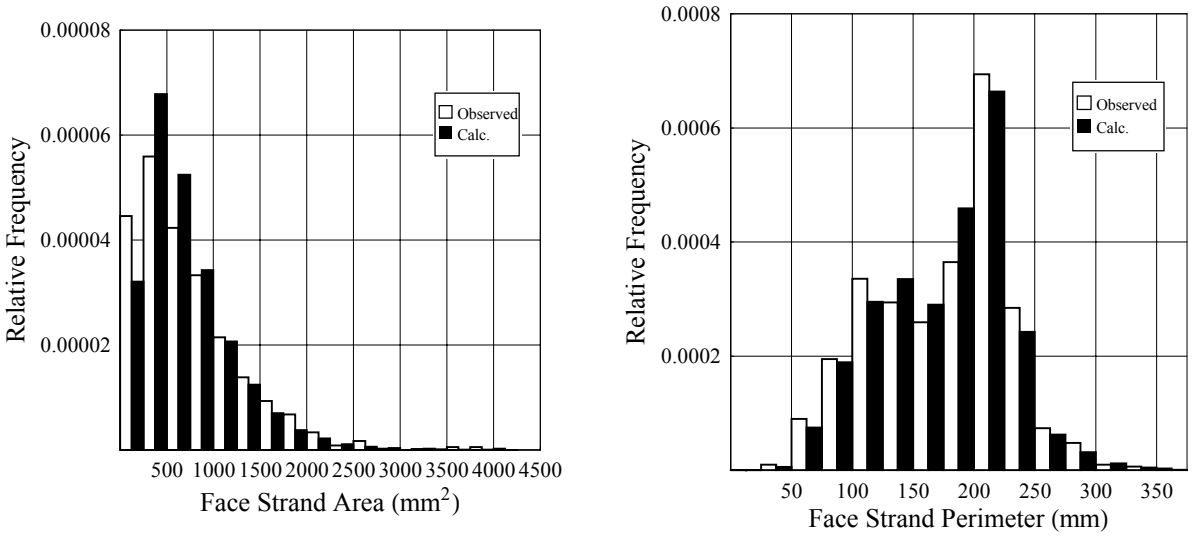

Figure 2.11. Calculated area and perimeter (face) versus measured area and perimeter distributions.

After establishing the probability density functions of the variables, the Monte Carlo simulation subroutines were checked by generating several arrays of 1000 density, thickness, length, and width data from the specified distributions. The simulation subroutines could successfully generate random variables from the three-parameter Gamma distributions.

Formal tests verified the accuracy of these subroutines, as demonstrated in Figure 2.10, where two initial data sets of length data are compared to the simulated values. Based on these results, the type and parameters of the probability distribution functions listed in Table 2.2 were incorporated into the mat formation simulation model to recreate the structure of a three-layer OSB mat.

2.5.2 General Validation of the Model

Table 2.3. shows the measured and simulated densities of five sample boards and the pooled data set. A paired t-test revealed at the 95% confidence level, that the means of the density data sets were not significantly different, meanwhile an F-test confirmed that the equal variance assumption was valid. Using the experimental and simulated pooled data sets the horizontal density distribution was further analyzed by creating histograms and fitting possible distribution functions to the data. The close agreement of the two density histograms is apparent (Figure 2.12). The fitting procedure provided the Weibull probability density function for each of the data sets with parameters given in Table 2.4. The result of the validation supported the feasibility of this simulation technique for the mat structure of oriented strand board. Although the validation was performed on a single-layer, randomly formed mat, the model is capable of describing the spatial characteristics of multi-layer oriented mats.

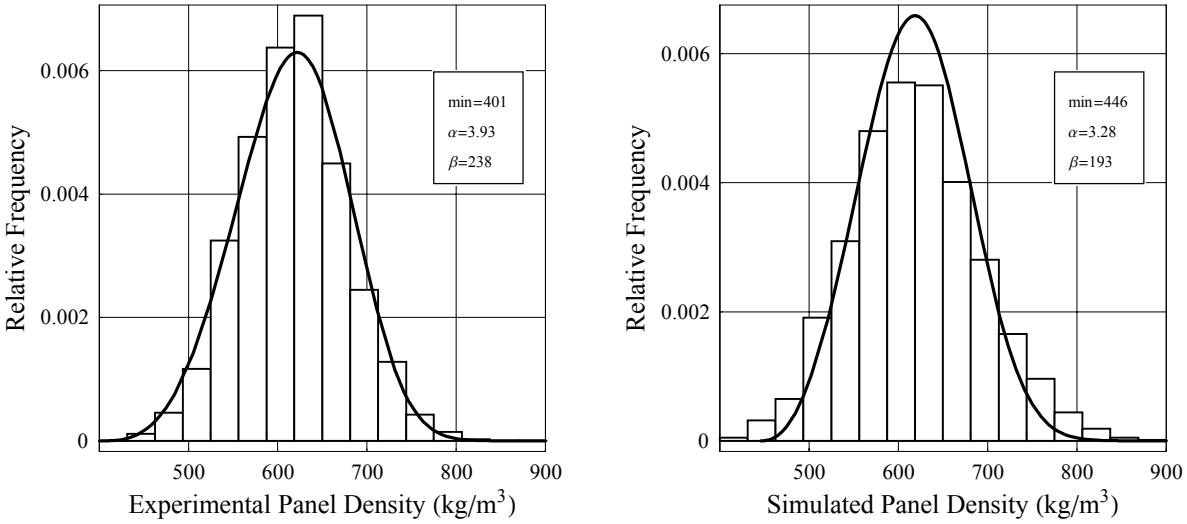

Figure 2.12. Density histograms generated from the experimental and predicted horizontal density data.

Table 2.3. Descriptive statistics of experimental and simulated board horizontal densities (RND Seed = random number generator initialization value).

(Target Density)	Experimental Results: (610 kg/m^3)						Simulation Results: (617.38 kg/m^3)					
[RND Seed]	1	2	3	4	5	Σ	1 [4617]	2 [2115]	3 [6203]	4 [8123]	5 [9235]	Σ
Mean (μ)	626.86	610.35	622.15	610.50	617.04	617.38	620.33	618.63	618.04	621.65	618.86	619.05
Stdev.(σ)	63.87	54.26	54.51	56.01	67.71	59.77	57.96	53.14	56.00	58.44	60.91	57.29
C.O.V. [%]	10.19	8.89	8.76	9.17	10.97	9.68	9.34	8.59	9.06	9.40	9.84	9.25
Min	484.95	457.52	467.51	441.46	399.90	399.90	469.86	482.27	485.27	446.34	473.01	446.34
Max	822.29	763.74	754.63	786.13	787.72	822.29	798.32	791.78	798.75	781.71	811.04	811.04

Table 2.4. Parameters of the fitted Weibull distributions (α_{stat}=0.05).

Horizontal Density Distribution	Parameters			Goodness-of-Fit Statistics						
	min.	α	β	d.o.f	χ^2	χ^2 (α_{stat}, d.o.f.)	p-value	K-S	K-S(α_{stat}, n)	p-value
Experiment	399	3.98	240	14	27.10	23.70	0.019	0.032	0.040	0.195
Simulation	446	3.28	193	14	15.00	23.70	0.380	0.022	0.038	0.574

2.5.3 Simulation of a Three-Layer Oriented Strand Board Mat

The main objective of the simulation program was to gain insight into the structure of a commercially produced OSB mat, thus forming the basis for a more thorough model of the hot-pressing process.

It is assumed that the rotation angle of the strands in the face and core layer follow a uniform probability distribution. After visual observation of a commercial OSB panel, the degree of alignment (limits on the orientation) of the strands on the face layer were determined to be ±40°. It was also assumed that the same restriction was applicable to the core layer. The mass proportion of the top, core, and bottom layers in the simulated mat was 1/4 : 1/2 : 1/4. The ratios were used to determine the weight fraction of the layers, in order to reach the final compressed density of 610 kg/m^3 (~38 lb/ft^3). Figure 2.13 depicts the result of the simulation together with the input parameters.

A fine mesh with an 18 mm grid density was superimposed on the simulated mat structure, and the properties of the mat were calculated at 676 grid points (26 x 26). The number of strands showed large differences among grid points ranging from 27 to 55 strands at different locations in the mat (Figure 2.14a). The strand thickness distribution is depicted with a contour map in Figure 2.14b. Notice that the thickness map is different from the strand number map, because the thickness was considered as a random variable.

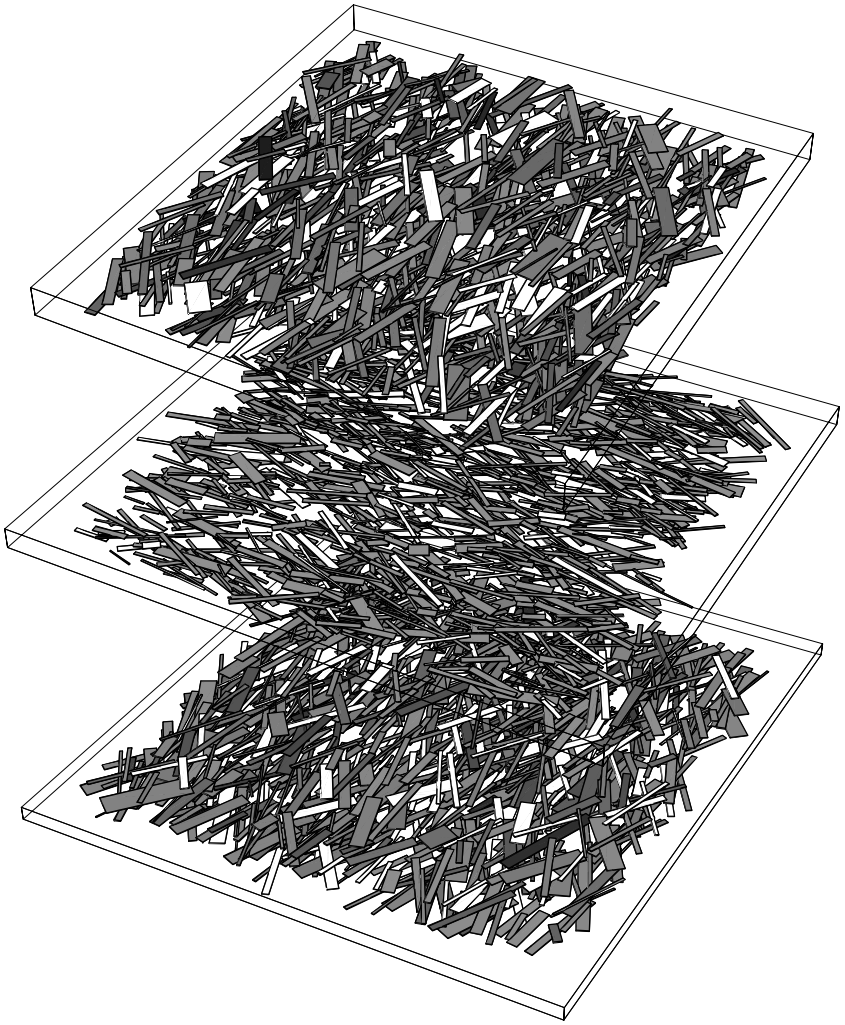

Top Layer	
Weight	655 g
Length	Empirical
Width	G(1.085, 2.280, 3.415)
Thickness	G(0.000, 8.690, 3.074)
Density	G(351.0, 2.340, 49.33)
Orientation	U(−40,40)
Flake #	3183
Core Layer	
Weight	1310 g
Length	Empirical
Width	G(0.788, 2.495, 2.165)
Thickness	G(0.015, 6.807, 0.085)
Density	G(310.0, 4.728, 34.671)
Orientation	U(50,130)
Flake #	13827
Bottom Layer	
Weight	655 g
Length	Empirical
Width	G(1.085, 2.280, 3.415)
Thickness	G(0.000, 8.690, 3.074)
Density	G(351.0, 2.340, 49.33)
Orientation	U(−40,40)
Flake #	3131

Figure 2.13. The reconstructed three-layer OSB mat (G=Gamma (min, α, β), U=Uniform (min, max). The mat area is 450 x 450 mm. The shade designates the density of the strands. The layers are separated with only a fraction of the flakes shown for better visualization.

a.)

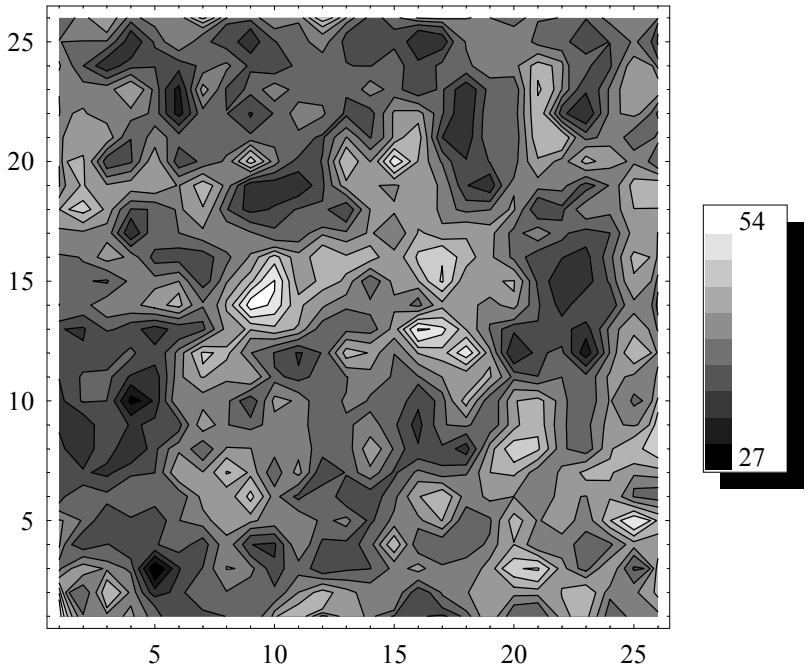

b.)

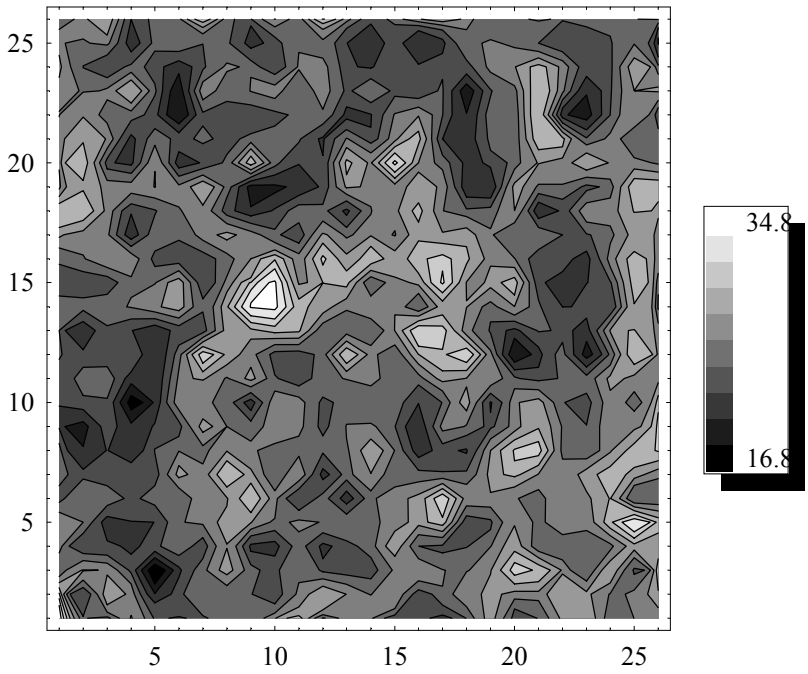

Figure 2.14. Contour map of the number (a.) and the total thickness (b.) of strands at the grid points. The distance between the grid points is 18 mm.

The mat was compressed to the final thickness with a simulated cold pressing process. The influence of temperature and moisture at this stage was ignored. Figure 2.15 shows the final horizontal density profile in the simulated three-layer OSB mat. The mean density (611.7 kg/m^3) showed good agreement with the intended target density of the board.

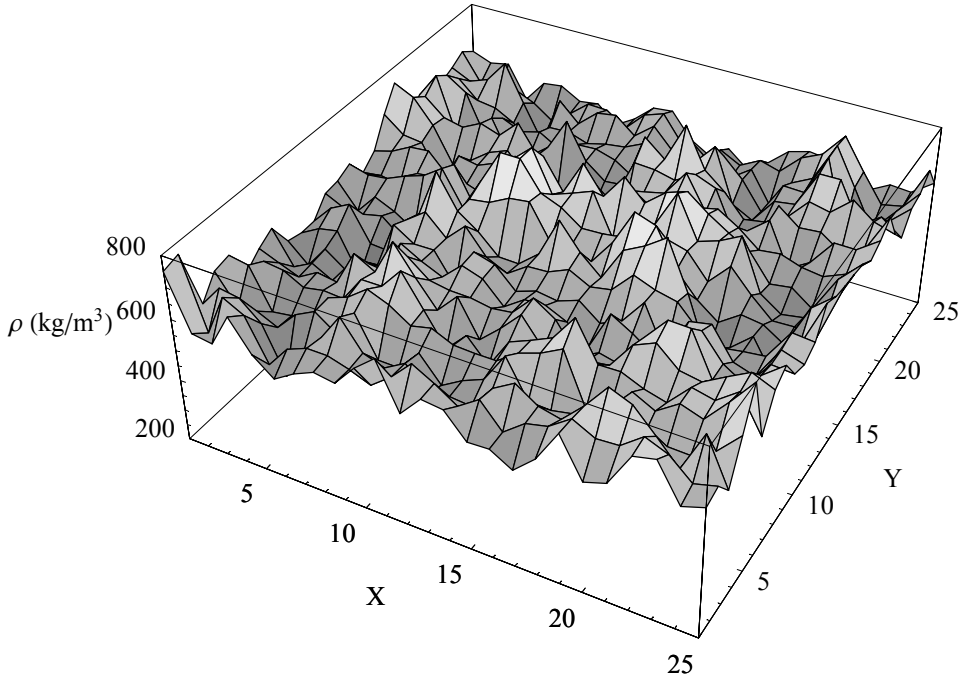

Figure 2.15. Predicted horizontal density distribution of the compressed mat at the grid points. The distance between the grid points is 18 mm. The average density is 611.7 kg/m^3.

One of the most important parameters related to the effectiveness of the bonding is the contact area between strands. Figure 2.16 shows the calculated contact area (C.A.), as a fraction of the total available strand area, versus the compression strain. Compression strain is defined as the ratio of the distance between the press platens and the uncompressed mat thickness. At the end of the press closure 93 % of the total strand area was in contact, which implied that at least 7 % of the strand area was not available for bonding.

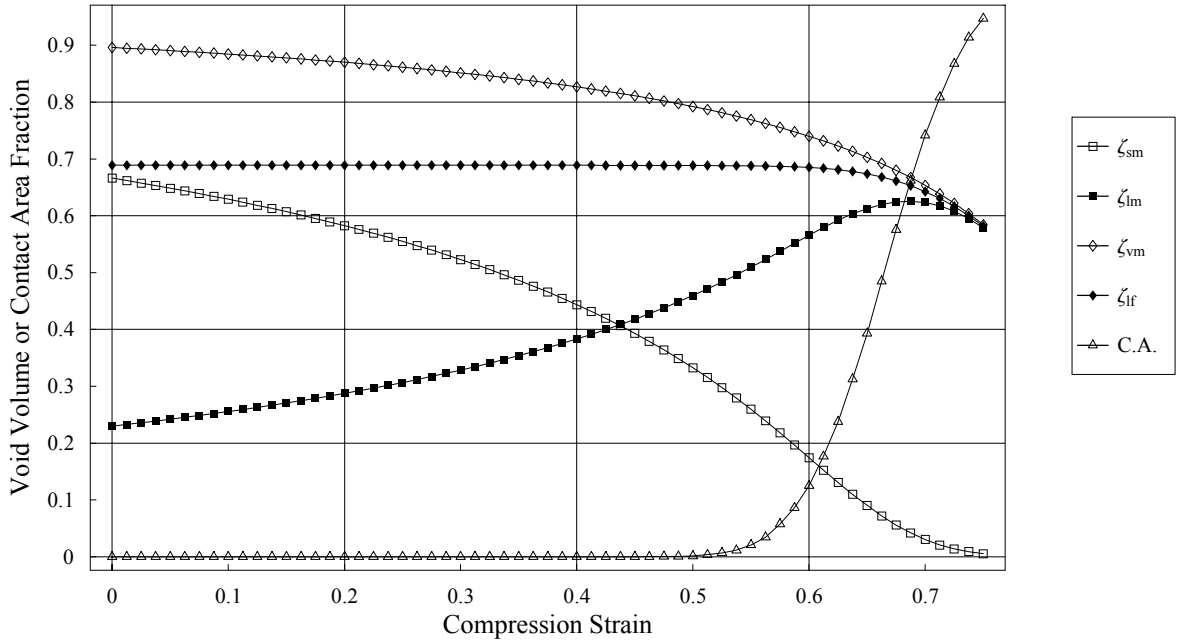

Figure 2.16. Simulated contact area and void volume as a function of mat compression strain.

Figure 2.16 summarizes the various void volume fractions as a function of the compression strain. In this example there is a thirty-fold decrease in space volume fraction (ζ_{sm}), which is the fraction of the volume of space between the flakes to the volume of the mat. As the majority of the space between the flakes is eliminated from the mat, the total void fraction (ζ_{vm}) approaches the fraction of lumen volume in the flakes (ζ_{lf}). The lumen fraction of the strands remains constant at the beginning of the pressing process, because the cellular structure of the flakes has not yet been compressed. The densification of the flakes was initiated when the mat was compressed to approximately half of its initial thickness.

Figure 2.17 shows the change of the density of the mat (ρ_m), and the density of the flakes (ρ_{fl}) during the compression process. The density of the mat is lower at the beginning of the pressing process than the density of the constituent flakes, due to the large amount of space present in the structure. As the mat is compressed the mat density immediately starts to increase and gets close to the strand density at the end of the compression. On the other hand, the mat has to be compressed to half of its thickness before continuous flake columns are formed, and the porous structure of the flakes is compressed. In this example, a compression strain of 0.5 marks the onset of flake density increase (ρ_f).

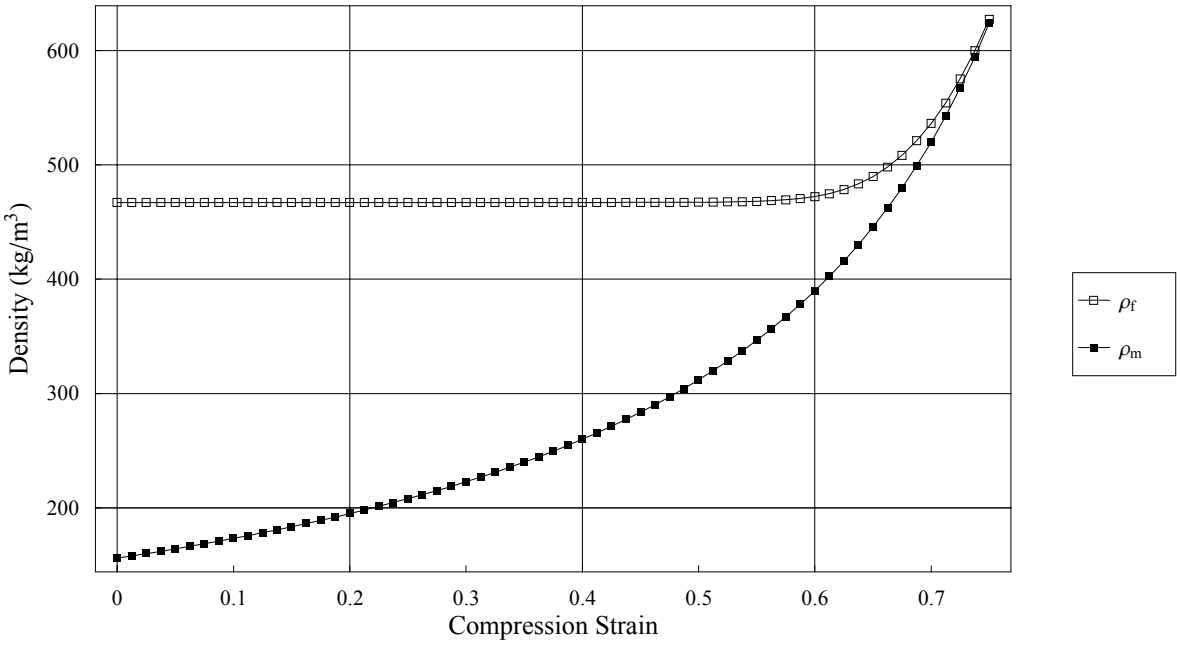

Figure 2.17. Simulated mat and flake density as a function of mat compression strain.

The void volume fractions and the mat density are closely related to the heat and mass transfer properties of the mat. For example, the thirty-fold change in space volume fraction has a great effect on the thermal conductivity, permeability, and diffusivity of the mat. It is apparent that the simulation of heat and mass transfer during the hot-pressing must take into consideration the structural dynamics of the mat during the press closure.

2.5.4 Simulation of a Random Fiber Network

The robustness of the model allows the simulation of not only OSB mats, but also other particle or fiber mat structures. For the purpose of illustration a fiberboard mat simulation was performed. It was assumed that each fiber dimension followed a truncated normal distribution, and the standard deviation was one quarter of the mean of the particular property. The mean fiber length was assumed to be 3.0 mm, and the mean width and thickness 0.035 mm, resulting in an approximate 1:100 diameter to length ratio. This is typical in the case of softwood longitudinal tracheids. The orientation angle of the fibers was unrestricted (random). Four hundred fibers were deposited on a 49 mm^2 area. Figure 2.18 shows the simulation outcome. It should be noted that the validation of this process for a fiberboard mat requires additional experimental work.

2.6 Conclusions

The proposed mat formation simulation model is capable of representing the three dimensional spatial structure of an uncompressed multi-layer wood-based composite mat using the parameters of experimentally determined distributions of strand properties. The model considers the dimensions of the strands, such as the length, width, and thickness as random variables. Additionally, a stochastic density value can be assigned to each strand, which allows the incorporation of the density variability represented by mixed species. None of the previously published models used probability density functions based on geometry and density data collected on industrial flakes. This makes possible a more accurate approximation of the horizontal density variation of the mat and the final panel.

The model can calculate such essential properties as the change of the strand contact area and several void volume fractions within the mat during the consolidation. The contact area is indicative of the effectively bonded area of the panel. The void volume fractions are related to the change in heat and mass transfer properties of the mat during the compression process.

Although the model was presented here to simulate the structure of an OSB mat, it is robust enough to describe the mat formation of a wide range of wood-based composites, from fiberboard to laminated strand lumber. With modifications, the proposed model is capable of incorporating the tilting and bridging, or the shape of the strands, which may improve the simulation results.

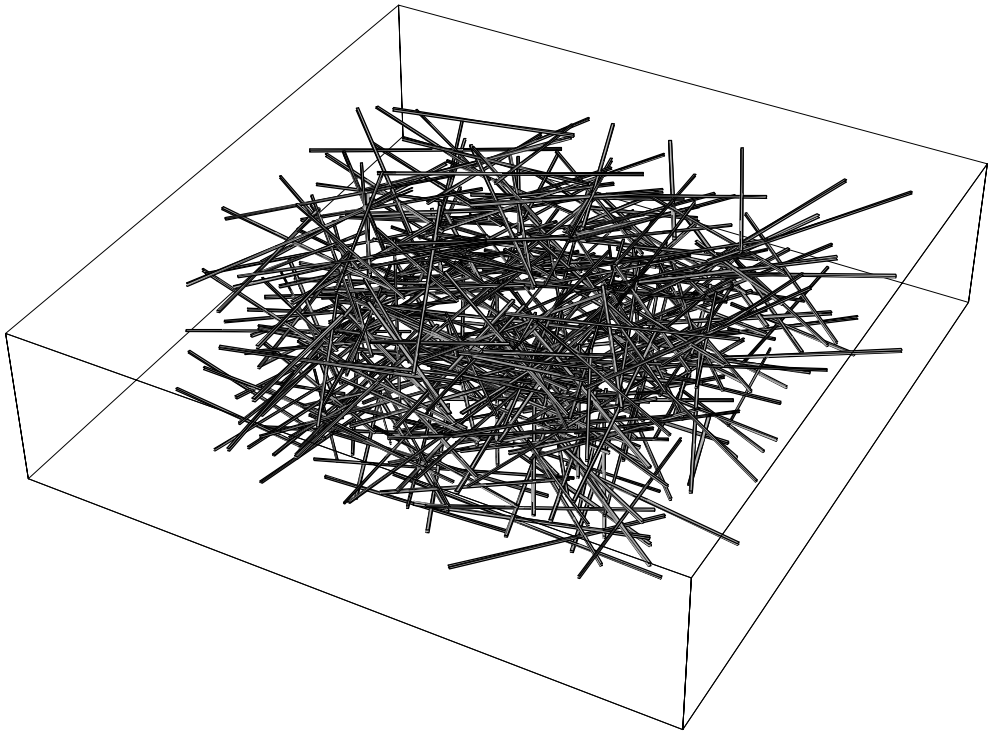

Simulation Parameters	
Fiber #	400
Length	N(3.0, 0.75)
Width	N(0.035, 0.00875)
Thickness	N(0.035, 0.00875)
Orientation	U(−180, 180)

Figure 2.18. The simulation results of the deposition of 400 fibers on a 7 x 7 mm area (N=Normal (μ, σ), U=Uniform(min, max)). The orientation of the fibers is unrestricted.

References

Bhagwat, S. 1971. Physical and mechanical variations in cottonwood and hickory flakeboards made from flakes of three sizes. Forest Prod. J. 21(9):101-103.

Brumbaugh, J. 1960. Effect of flake dimension on properties of particleboard. Forest Prod. J. (5):243-246.

Dai, C., P. R. Steiner. 1993. Compression behavior of randomly formed wood flake mats. Wood and Fiber Science 25(4):349-358.

Dai, C., P. R. Steiner. 1994.a. Spatial structure of wood composites in relation to processing and performance characteristics. Part II. Modeling and simulation of a randomly-formed flake layer network. Wood Sci. and Technol. (28):135-146.

Dai, C., P. R. Steiner. 1994.b. Spatial structure of wood composites in relation to processing and performance characteristics. Part III. Modeling the formation of multi-layered random flake mats. Wood Sci. and Technol. (28):229-239.

Heebink, B. G., R. A. Hann. 1959. How wax and particle shape affect the stability and strength of oak particleboards. Forest Prod. J. 9(7):197-203.

Hoglund, H., U. Sholin, G. Tistad. 1976. Physical properties of wood in relation to chip refining. Tappi 59(6):144-147.

Kallmes, O. J. 1961. The application of probability theory to papermaking. Tappi 44(7):516-519.

Kallmes, O. J., H. Corte. 1960. The structure of paper. Part I. The statistical geometry of an ideal two dimensional fiber network. Tappi 43(9):737-752.

Kallmes, O. J., H. Corte, G. Bernier. 1961. The structure of paper. Part II. The statistical geometry of a multiplanar fiber network. Tappi 44(7):519-528.

Kelley, M. W. 1977. Critical literature review of relationships between processing parameters and physical properties of particleboard. U.S.D.A. Forest Service, Forest Products Laboratory, General Technical ReportFPL-10

Lang, M. E., M. P. Wolcott. 1995. Modeling the consolidation of wood-strand mat. AMD-Vol. 209/MD-Vol. 60, Mechanics of Cellulosic Materials. ASME 1995.

Lang, M. E., M. P. Wolcott. 1996a. A model for viscoelastic consolidation of wood-strand mats. Part I. Structural characterization of the mat via Monte Carlo simulation. Wood and Fiber Science 28(1):100-109.

Lang, M. E., M. P. Wolcott. 1996b. A model for viscoelastic consolidation of wood-strand mats. Part II. Static stress-strain behavior of the mat. Wood and Fiber Science 28(3):369-379.

Law, A. M., W. D. Kelton. 1982. Simulation Modeling and Analysis. McGraw Hill Book Company, New York, NY.

O'Rourke, J. 1994. Computational Geometry in C. Cambridge University Press, Cambridge, England

Steiner, P. R., C. Dai. 1993. Spatial structure of wood composites in relation to processing and performance characteristics. Part I. Rationale for model development. Wood Sci. and Technol. (28):45-51.

Strickler, M. D. 1959. Effects of press cycle and moisture content on properties of douglas-fir flakeboard. Forest Prod. J. 9(7):203-215.

Suchsland, O. 1959. An analysis of the particle board process. Michigan Quarterly Bulletin 42(2):350-372.

Suchsland, O. 1962. The density distribution in flake boards. Michigan Quarterly Bulletin 45(1):104-121.

Suchsland, O. 1967. Behavior of particleboard mat during the press cycle. Forest Prod.J.17(2):51-57.

Suchsland, O., H. Xu. 1989. A simulation of the horizontal density distribution in a flakeboard. Forest Prod. J. 39(5):29-33.

Suchsland, O., X. Hong. 1989. Model analysis of flakeboard variables. Forest Prod. J. 41(11/12):55-60.